STRUCTURAL BIOLOGY COMMUNICATIONS

ISSN 2053-230X

Structure–activity correlations for three pyrido[2,3-*d*]pyrimidine antifolates binding to human and *Pneumocystis carinii* dihydrofolate reductase

Vivian Cody,[a,b]* Jim Pace,[a] Ojas A. Namjoshi[c] and Aleem Gangjee[c]

[a]Structural Biology Department, Hauptman-Woodward Medical Research Institute, 700 Ellicott Street, Buffalo, NY 14203, USA, [b]Structural Biology Department, School of Medicine and Biomedical Sciences, University at Buffalo, 700 Ellicott Street, Buffalo, NY 14203, USA, and [c]Division of Medicinal Chemistry, Graduate School of Pharmaceutical Sciences, Duquesne University, Pittsburgh, PA 15213, USA. *Correspondence e-mail: cody@hwi.buffalo.edu

Received 27 February 2015
Accepted 29 April 2015

Edited by R. A. Pauptit, Macclesfield, England

Keywords: dihydrofolate reductase; *Pneumocystis carinii*; pathogens; antifolate inhibitors; conformational analysis.

PDB references: human dihydrofolate reductase, complex with pyrido[2,3-*d*]pyrimidine inhibitor, 4qhv; 4qjc; *Pneumocystis carinii* dihydrofolate reductase, complex with pyrido[2,3-*d*]pyrimidine inhibitor, 4qjz

Supporting information: this article has supporting information at journals.iucr.org/f

To further define the interactions that enhance the selectivity of binding and to directly compare the binding of the most potent analogue {N^6-methyl-N^6-(3,4,5-trifluorophenyl)pyrido[2,3-*d*]pyrimidine-2,4,6-triamine; compound **26**} in the series of bicyclic pyrido[2,3-*d*]pyrimidine analogues of piritrexim (PTX) with native human (h), *Pneumocystis carinii* (pc) and *Pneumocystis jirovecii* (pj) dihydrofolate reductase (DHFR) enzymes, the crystal structures of hDHFR complexed with N^6-methyl-N^6-(4-isopropylphenyl)pyrido[2,3-*d*]pyrimidine-2,4,6-triamine (compound **22**), of hDHFR complexed with compound **26** and of pcDHFR complexed with N^6-methyl-N^6-1-naphthylpyrido[2,3-*d*]pyrimidine-2,4,6-triamine (compound **24**) are reported as ternary complexes with NADPH. This series of bicyclic pyrido[2,3-*d*]pyrimidines were designed in which there was a transposition of the 5-methyl group of PTX to the N9 position of the pyrido[2,3-*d*]pyrimidine. It was hypothesized that the N9-methyl group would preferentially interact with Ile123 of pcDHFR (and Ile123 of pjDHFR), but not with the shorter Val115 in hDHFR. Structure–activity data for this series of antifolates revealed that a trifluoro derivative (**26**) was the most selective against pjDHFR compared with mammalian DHFR (h/pj = 35.7). Structural data for the hDHFR–**26** complex revealed that **26** binds in a different conformation from that observed in the pcDHFR–**26** complex. In the hDHFR–**26** complex the trifluorophenyl ring of **26** occupies a position near the cofactor-binding site, with close intermolecular contacts with Asp21, Ser59 and Ile60, whereas this ring in the pcDHFR–**26** complex is positioned away from the cofactor site and near Ile65, with weaker contacts with Ile65, Phe69 and Ile123. Comparison of the intermolecular contacts between the N9-methyl group with Val115/Ile123 validates the hypothesis that the N9-methyl substituent preferentially interacts with Ile123 compared with Val115 of hDHFR, as the weaker contact with Val115 in the hDHFR structure is consistent with its weaker binding affinity compared with pcDHFR. The results for the structures of hDHFR–**22** and pcDHFR–**24** show that their inhibitor-binding orientation is similar to that observed in pcDHFR–**26** and the pcDHFR variant (F69N) reported previously. The naphthyl moiety of **24** makes several intermolecular contacts with the active-site residues in pcDHFR that help to stabilize the binding, resulting in a more potent inhibitor.

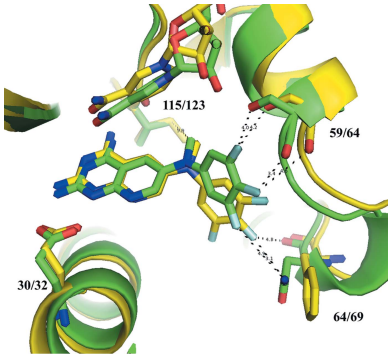

1. Introduction

A novel series of bicyclic pyrido[2,3-*d*]pyrimidines that contain an N^6-(substituted phenyl)pyrido[2,3-*d*]pyrimidine-2,4,6-triamine scaffold in which the substituted aniline is directly attached to the 6-position of the pyrido[2,3-*d*]

Table 1
Crystal data for the antifolates under study.

Values in parentheses are for the highest resolution shell.

	hDHFR–**22**–NADPH	hDHFR–**26**–NADPH	pcDHFR–**24**–NADPH
PDB code	4qhv	4qjc	4qjz
Data collection			
Space group	*H*3	*H*3	$P2_1$
Unit-cell parameters			
a (Å)	84.4	84.5	36.7
b (Å)	84.4	84.5	42.9
c (Å)	78.3	77.9	61.0
α (°)	90.0	90.0	90.0
β (°)	90.0	90.0	95.3
γ (°)	120.0	120.0	90.0
Beamline	11-1, SSRL	11-1, SSRL	11-1, SSRL
Resolution (Å)	34.5–1.54 (1.62–1.54)	34.4–1.54 (1.62–1.54)	35.0–1.61 (1.72–1.61)
Wavelength (Å)	0.975	0.975	0.975
R_{merge}† (%)	0.026 (0.79)	0.062 (0.75)	0.050 (0.70)
Completeness (%)	92.8 (75.4)	96.3 (83.0)	95.8 (97.0)
Observed reflections	72513 (7697)	97495 (9939)	61131 (9036)
Unique reflections	28762 (3398)	29910 (3757)	23617 (3467)
$\langle I/\sigma(I)\rangle$	21.3 (4.5)	10.2 (1.2)	12.6 (1.5)
Multiplicity	2.5 (2.3)	3.3 (2.6)	2.6 (2.6)
Refinement model			
Resolution (Å)	34.5–1.54	34.4–1.54	35.0–1.61
No. of reflections	24506	24614	22409
R factor‡	0.178	0.183	0.204
R_{free}§	0.222	0.217	0.244
Total protein atoms	1757	1678	1851
Total waters	154	105	73
Average *B* factor (Å^2)	19.1	23.2	22.3
R.m.s.d. from ideal			
Bond lengths (Å)	0.025	0.026	0.02
Bond angles (°)	2.85	2.52	2.19
Luzzati plot error (Å)	0.168	0.218	0.205
Ramachandran plot (%)			
Most favored	98.4	98.4	95.5
Additional allowed	1.1	1.6	3.0
Generously allowed	0.5	0.0	1.5
Disallowed	0.0	0.0	0.0

† $R_{merge} = \sum_{hkl}\sum_i |I_i(hkl) - \langle I(hkl)\rangle| / \sum_{hkl}\sum_i I_i(hkl)$, where $\langle I(hkl)\rangle$ is the mean intensity of a set of equivalent reflections. ‡ *R* factor = $\sum_{hkl} ||F_{obs}| - |F_{calc}|| / \sum_{hkl} |F_{obs}|$, where F_{obs} and F_{calc} are observed and calculated structure-factor amplitudes, respectively. § R_{free} was calculated as for the *R* factor for a random 5% subset of all reflections.

pyrimidine ring have been shown to be selective and potent inhibitors of pathogenic sources of dihydrofolate reductase (DHFR) such as *Pneumocystis jirovecii*, a causative agent of pneumonia in HIV/AIDS patients (Gangjee *et al.*, 2013). These compounds are analogues of piritrexim (PTX), a potent but nonselective DHFR inhibitor (Grivsky *et al.*, 1980; Kovacs *et al.*, 1988; Falloon *et al.*, 1990). Of note are a series of analogues in which the 5-methyl group of PTX was transposed to the N9 position of the pyrido[2,3-*d*]pyrimidine. It was hypothesized that the N9-methyl group would make favorable contacts with Ile123 of pcDHFR (and Ile123 of pjDHFR), but not with the shorter Val115 of human DHFR. Structure–activity data for the inhibition of pyrido[2,3-*d*]pyrimidines against hDHFR, pcDHFR and pjDHFR enzymes revealed that a trifluro derivative (compound **26**; Fig. 1) was the most selective against pjDFHR compared with the mammalian DHFR (IC_{50} of 0.0042 μM for pjDFHR compared with 0.15 μM for hDHFR), with a selectivity ratio of 35 (Gangjee *et al.*, 2013).

To further define the interactions that enhance the selectivity of binding and to directly compare the binding of the most potent analogue in the series, N^6-methyl-N^6-(3,4,5-trifluorophenyl)pyrido[2,3-*d*]pyrimidine-2,4,6-triamine (compound **26**), with native hDHFR, pcDHFR and pjDHFR, we report crystal structure data for hDHFR in complex with N^6-methyl-N^6-(4-isopropylphenyl)pyrido[2,3-*d*]pyrimidine-2,4,6-triamine (compound **22**), hDHFR in complex with **26** and pcDHFR in complex with N^6-methyl-N^6-1-naphthylpyrido[2,3-*d*]pyrimidine-2,4,6-triamine (compound **24**) as ternary complexes with NADPH. Additionally, we report the IC_{50} binding affinity of N^6-methyl-N^6-phenylpyrido[2,3-*d*]pyrimidine-2,4,6-triamine (compound **16**) and **26** (Fig. 1) against the double variant F69N/K37S of pcDHFR, the crystal structure of which has previously been reported, in order to verify that the activity of the variant was not significantly different from that of the native enzyme; a question that had been raised by reviewers (Gangjee *et al.*, 2013).

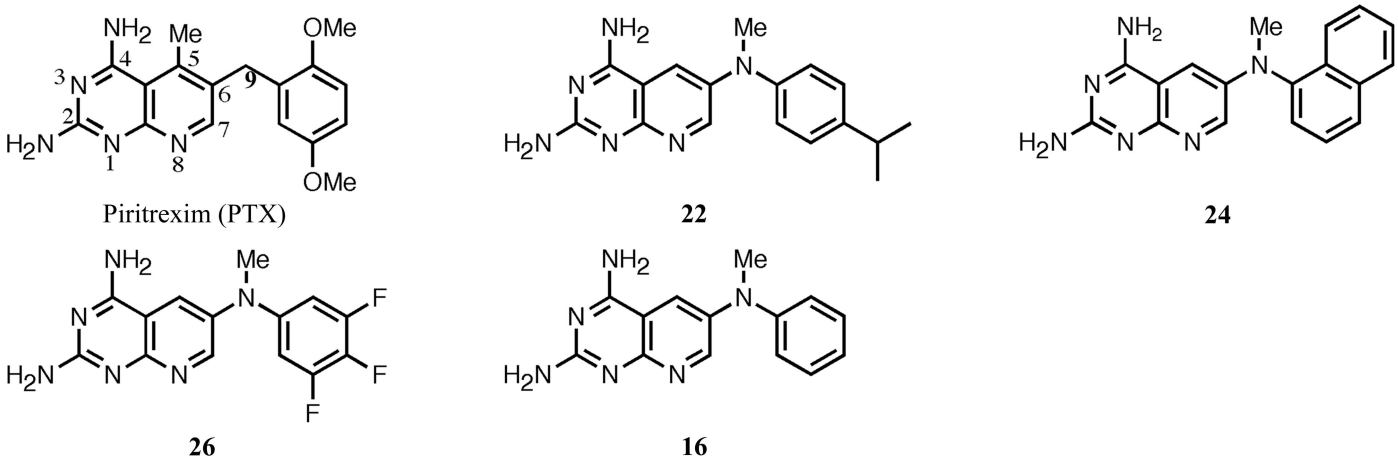

Figure 1
Schematics of the pyrido[2,3-*d*]pyrimidines under study. The numbers correspond to those used in Gangjee *et al.* (2013).

Table 2
Comparison of F-atom contacts and bridge torsion angles for inhibitor **26**.

hDHFR–**26**		pcDHFR–**26**	
Trifluoro contacts (Å)			
3′F···Asp21 carbonyl	3.5	3′F···Ile65 CG2	3.9
4′F···Ser59 carbonyl	3.4	4′F···Phe69 CE	5.8
5′F···Ile60 CG	3.9	5′F···Ile123 CD1	6.9
Bridge conformation (°)			
C7—C6—N9—C1′	−3.9	C7—C6—N9—C1′	33.2
C6—N9—C1′—C6′	63.2	C6—N9—C1′—C6′	45.9
C7—C6—N9—CH_3	−167.0	C7—C6—N9—CH_3	−152.0

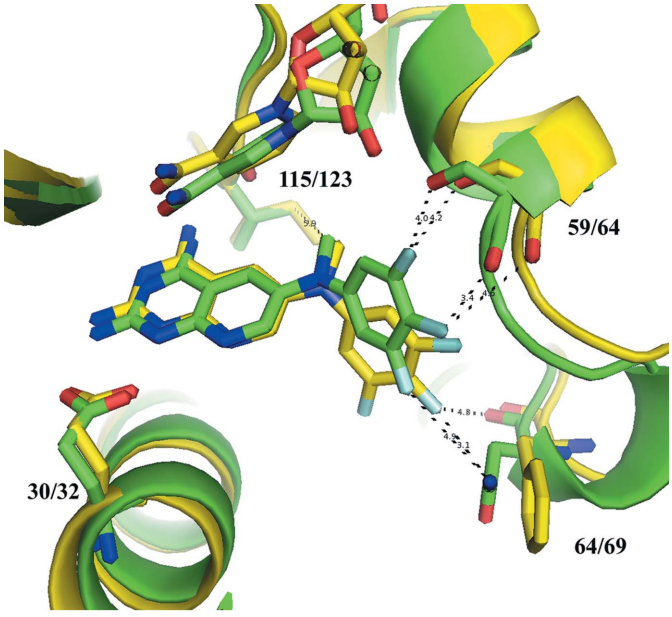

(*a*)

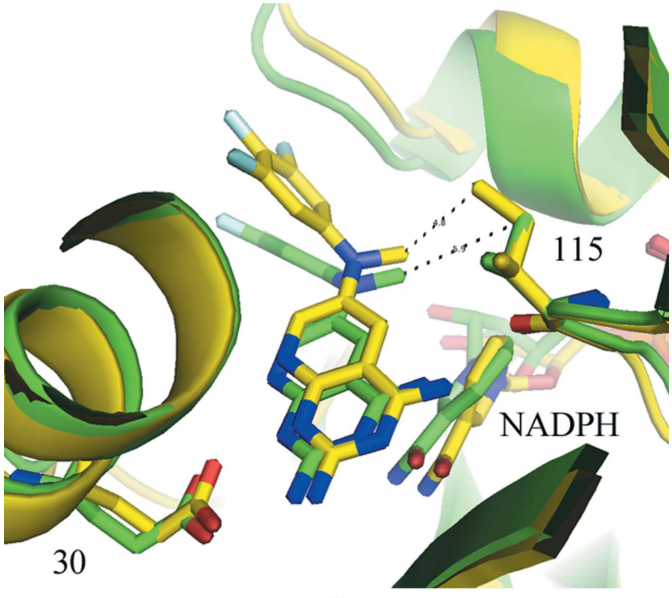

(*b*)

Figure 2
(*a*) Comparison of the contacts of the 3′,4′,5′-trifluoro atoms with the side chains of Ser59/64 and Asn64/Phe69 for hDHFR and pcDHFR, respectively. (*b*) Comparison of the binding of **26** in hDHFR (green; PDB entry 4qjc) and pcDHFR (yellow; PDB entry 4ixe; Gangjee *et al.*, 2013), highlighting the contacts of the N9-methyl group with Val115 and Ile123 in hDHFR and pcDHFR, respectively.

Table 3
Contacts (Å) involving the inhibitor N9 CH_3 with Val115 (hDHFR) or Ile123 (pcDHFR), Thr56 (hDHFR) or Thr61 (pcDHFR), and Ile60 (hDHFR) or Ile65 (pcDHFR).

The shortest distances for each complex are given for comparison.

DHFR	N9 CH_3···Val115/Ile123	N9 CH_3··· Thr56/Thr61	N9 CH_3··· Ile60/Ile65
hDHFR–**22**	Carbonyl O, 5.3; CG1, 6.9	CG2, 4.6	CG1, 4.5
pcDHFR–**22** (F69N)	Carbonyl O, 4.7; CG1, 4.8	CG2, 3.8	CG1, 4.7
hDHFR–**26**	Carbonyl O, 5.2; CG2, 5.8	CG2, 3.9	CG1, 4.5
pcDHFR–**26**	Carbonyl O, 4.5; CG1, 5.4	CG2, 3.6	CG1, 5.2
pcDHFR–**24**	Carbonyl O, 4.5; CD1, 4.3	CG2, 3.6	CG1, 4.2

2. Methods

2.1. Crystallization

Recombinant hDHFR (Gangjee *et al.*, 2009) and pcDHFR (Gangjee *et al.*, 2013) were expressed and purified as described previously. The hDHFR protein was washed in a Centricon-10 with 100 m*M* K_2HPO_4 buffer pH 6.9 with 30% saturated ammonium sulfate and concentrated to 7.9 mg ml^{-1}, and the pcDHFR protein was washed with 50 m*M* MES buffer pH 6.0, 100 ml KCl and concentrated to 11.4–14.1 mg ml^{-1}. All DHFR samples were incubated for 1 h on ice with a tenfold excess of NADPH and compounds **22**, **24** and **26**, respectively, prior to crystallization using the hanging-drop vapor-diffusion method using siliconized glass cover slips and storage at 14°C. Protein droplets of the hDHFR complexes contained K_2HPO_4 pH 6.9 with 30% saturated ammonium sulfate equilibrated against a reservoir solution consisting of 100 m*M* K_2HPO_4 buffer pH 6.9 with 60% saturated ammonium sulfate, 3%(*v*/*v*) ethanol, while the protein droplets for the pcDHFR complex consisted of 35% PEG 2K, 49 m*M* MES pH 6.0, 100 m*M* KCl equilibrated against a reservoir solution consisting of 0.1 *M* HEPES pH 7.5, 25% PEG 2000 MME. Crystals of the pcDHFR–**24**–NADPH ternary complex were monoclinic and belonged to space group $P2_1$. The crystals of the two hDHFR complexes were hexagonal and belonged to space group *H*3. Data were collected at 100 K to between 1.54 and 1.62 Å resolution for the three DHFR complexes using the remote-access robot on beamline 11-1 at the Stanford Synchrotron Radiation Laboratory (SSRL; Cohen *et al.*, 2002; González *et al.*, 2008; McPhillips *et al.*, 2002). The data for these crystals were processed using the *XDS* program package (Kabsch, 2010). The diffraction statistics are shown in Table 1.

2.2. Structure solutions

The three structures were solved by molecular-replacement methods using the coordinates of pcDHFR (PDB entry 4ixe; Gangjee *et al.*, 2013) for the pcDHFR complex and those of hDHFR (PDB entry 1u72; Cody *et al.*, 2005) for the two hDHFR complexes in *MOLREP* (Vagin & Teplyakov, 2010). Inspection of the resulting difference electron-density maps was made using *Coot* (Emsley *et al.*, 2010) running on an iMac workstation and revealed density for the ternary complex in all three crystals. Refinement was carried out using *REFMAC*5 (Murshudov *et al.*, 2011) in the *CCP*4 suite of programs (Winn

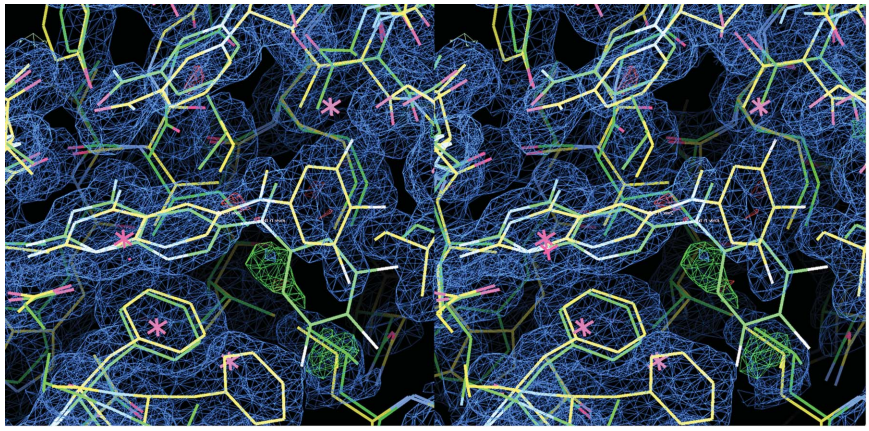

Figure 3
Stereo comparison of the $2F_o - F_c$ difference electron-density map (1σ) for the hDHFR–**26**–NADPH ternary complex (yellow) with the fit of the pcDHFR–**26**–NADPH complex (green). Also shown is the 3.5σ $F_o - F_c$ density (green), which has a partial fit for an alternate conformation of the trifluorophenyl ring as observed in the pcDHFR complex (green).

et al., 2011). The Ramachandran conformational parameters, based on the last refinement cycle, were generated by *RAMPAGE* (Lovell *et al.*, 2002) and showed that more than 96% of the residues have the most favored conformation and that none are in disallowed regions. Coordinates for these structures have been deposited in the Protein Data Bank (hDHFR–**22**, PDB entry 4qhv; hDHFR–**26**, PDB entry 4qjc; pcDHFR–**24**, PDB entry 4qjz).

3. Results

The crystal structures of three pyrido[2,3-*d*]pyrimidine antifolates (**22**, **24** and **26**; Fig. 1) are reported here as ternary complexes with either native human or native *P. carinii* DHFR in an effort to correlate their structure–activity relationships. These complexes are compared with previously reported complexes with inhibitors **16**, **22** and **26** (Fig. 1) with variant pcDHFR (Gangjee *et al.*, 2013).

Analysis of the crystal structure of the hDHFR–**26**–NADPH ternary complex reported here reveals differences in the binding geometry of **26** from that in the pcDHFR–**26**–NADPH complex (Gangjee *et al.*, 2013; Fig. 2, Table 2). The trifluorophenyl ring of **26** in the hDHFR complex occupies a pocket closer to the cofactor-binding site such that the 3′,4′,5′-trifluoro atoms make close intermolecular contacts with residue Ser59, whereas the trifluoro atoms make weaker contacts with the side chain of Phe69 in the pcDHFR–**26**–NADPH ternary complex (Fig. 2*a*; Table 2; Gangjee *et al.*, 2013). Differences in the binding geometry of compound **26** with both hDHFR and pcDHFR are also highlighted in Table 2.

Comparison of the intermolecular contacts between the N9-methyl group and Val115/Ile123 validates the hypothesis that the N-methyl substituent interacts with Ile123 preferentially compared with the shorter Val115 in hDHFR (Fig. 2*b*). These data show that the intermolecular contact between the N9-methyl group and Ile123 (4.8 Å) in pcDHFR is shorter than the contact in hDHFR (Val115, 5.9 Å; Table 3). The weaker contact in the hDHFR structure is consistent with its weaker binding affinity compared with pjDHFR. However, the weaker binding of pcDHFR compared with hDHFR suggests that this contact does not tell the complete story.

Interestingly, analysis of the $2F_o - F_c$ electron-density map of the hDHFR complex reveals a trace of positive density (3.5σ) that is occupied by the trifluorophenyl ring in the pcDHFR complex (Fig. 3). During refinement, a partial occupancy model of the trifluorophenyl ring in two alternate conformations was refined to incorporate this density; however, there was insufficient density to build up the rest of the phenyl ring to warrant accepting this as a final model. Additionally, the final refinement has the cofactor NADPH present at half-occupancy, with the phosphate positions in the backbone of the cofactor also occupied by sulfate from the crystallization medium.

The data for hDHFR–**22**–NADPH shows that the binding of compound **22** is similar to that observed in pcDHFR-F69N–

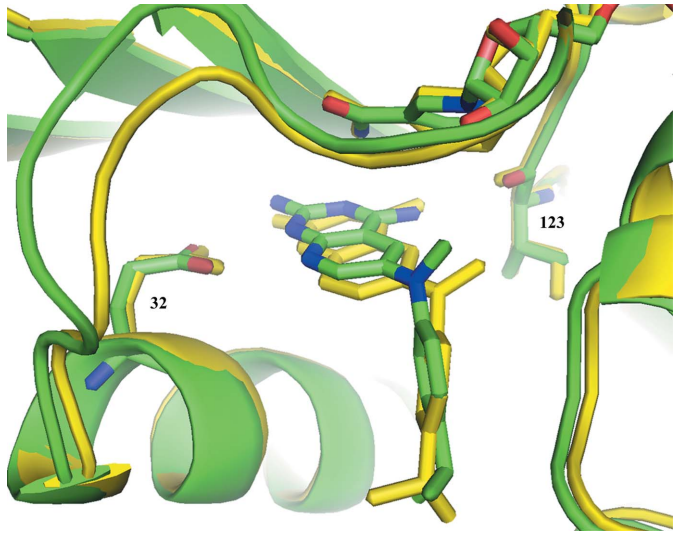

Figure 4
Comparison of hDHFR–**22**–NADPH (green; PDB entry 4qhv) with pcDHFR-F69N–**22**–NADPH (yellow; PDB entry 4ixf; Gangjee *et al.*, 2013), highlighting the contact of the N9-methyl group with Val115 (green) and Ile123 (yellow) of the pcDHFR complex.

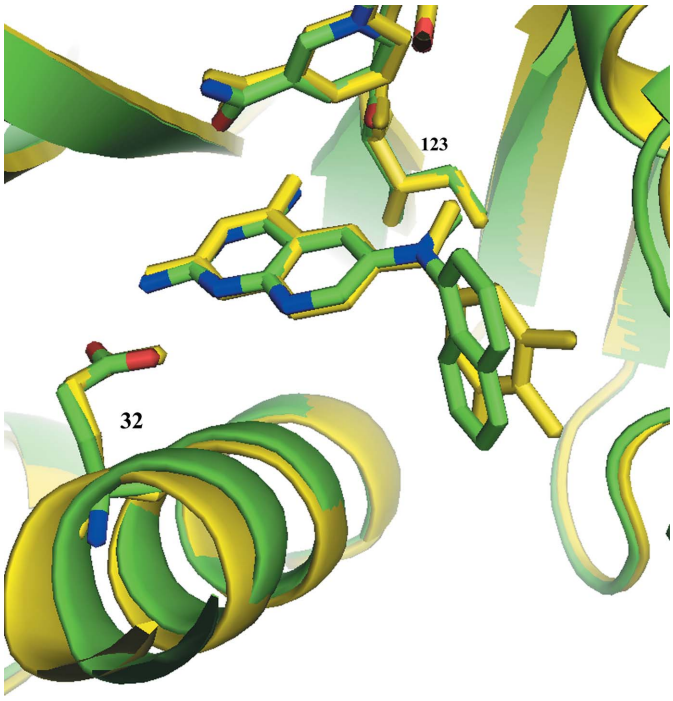

Figure 5
Comparison of pcDHFR–**24**–NADPH (green; PDB entry 4qjz) with pcDHFR–**26**–NAPDH (yellow; PDB entry 4ixe; Gangjee *et al.*, 2013).

22–NADPH (Gangjee *et al.*, 2013). The small variation in the conformation about the N9-methyl bridge results in a much weaker contact between the N9-methyl group and Val115 (7.1 Å) in the hDHFR complex than the same contact to Ile123 (4.8 Å) in the pcDHFR-F69N complex (Fig. 4). These structural results are consistent with the activity of **22** against hDHFR and pcDHFR. Unlike compounds **24** and **26**, there are few interactions of the 4-propyl group with the active-site residues.

Analysis of the structural data for the pcDHFR–**24**–NADPH ternary complex indicates that the binding orientation of **24** is similar to that in pcDHFR–**26**–NADPH (Fig. 5) and that the contact of the N9-methyl group is the shortest (4.4 Å) of the pcDHFR complexes in this series. These data show that the naphthyl moiety makes several intermolecular contacts with 4.5 Å of the side chains of residues Phe69, Pro66, Ile65 and Ile33. These hydrophobic interactions help stabilize the binding.

Activity data for the pcDHFR F69N/K37S double variant reveal that there is a slight decrease in binding affinity of **16** for the variant (IC_{50} of 0.10 and 0.076 μ*M* for mutant and wild-type pcDHFR, respectively), whereas there is an increase in the binding affinity of **26** for the pcDHFR variant (IC_{50} of 0.094 and 0.23 μ*M* for mutant and wild-type pcDHFR, respectively). However, these differences in IC_{50} are not significant. These data suggest that the F69N/K37S variants do not have a significant influence on binding kinetics and that the crystal structures of these variants (Gangjee *et al.*, 2013) is representative of the binding to the native DHFR enzyme.

4. Discussion

The crystal structures of three pyrido[2,3-*d*]pyrimidine antifolates are reported in complex with either human or *P. carinii* DHFR in an effort to understand their structure–activity relationships. The activity data reported for these analogues (Gangjee *et al.*, 2013), as well as for a variant form of pcDHFR (F69N/K37S), revealed that compound **26** was 35-fold more selective for binding *P. jirovecii* DHFR (pjDHFR) than the human enzyme. These structural results validate the hypothesis that the N9-methyl group interacts more favorably with Ile123 (present in both pcDHFR and pjDHFR) than with Val115 in hDHFR. These contacts range from 4.4 to 4.8 Å for pcDHFR and from 5.9 to 7.1 Å for hDHFR (Table 3).

Structure–activity correlations are more difficult to evaluate based on other active-site interactions. These data reveal that enzyme inhibition is at least tenfold greater for pjDHFR than for pcDHFR and that inhibition is somewhat weaker for hDHFR. The one anomaly is the potency of **24** with hDHFR.

Acknowledgements

This work was supported in part by National Institutes of Health Institute of Allergy and Infectious Diseases grant AI069966 (AG) and by the Greater Buffalo Community Foundation (VC).

References

Cody, V., Luft, J. R. & Pangborn, W. (2005). *Acta Cryst.* D**61**, 147–155.
Cohen, A. E., Ellis, P. J., Miller, M. D., Deacon, A. M. & Phizackerley, R. P. (2002). *J. Appl. Cryst.* **35**, 720–726.
Emsley, P., Lohkamp, B., Scott, W. G. & Cowtan, K. (2010). *Acta Cryst.* D**66**, 486–501.
Falloon, J. *et al.* (1990). *Clin. Res.* **38**, 361A.
Gangjee, A., Li, W., Lin, L., Zeng, Y., Ihnat, M., Warnke, L. A., Green, D. W., Cody, V., Pace, J. & Queener, S. F. (2009). *Bioorg. Med. Chem.* **17**, 7324–7336.
Gangjee, A., Namjoshi, O. A., Raghavan, S., Queener, S. F., Kisliuk, R. L. & Cody, V. (2013). *J. Med. Chem.* **56**, 4422–4441.
González, A., Moorhead, P., McPhillips, S. E., Song, J., Sharp, K., Taylor, J. R., Adams, P. D., Sauter, N. K. & Soltis, S. M. (2008). *J. Appl. Cryst.* **41**, 176–184.
Grivsky, E. M., Lee, S., Sigel, C. W., Duch, D. S. & Nichol, C. A. (1980). *J. Med. Chem.* **23**, 327–329.
Kabsch, W. (2010). *Acta Cryst.* D**66**, 125–132.
Kovacs, J. A., Allegra, C. J., Swan, J. C., Drake, J. C., Parrillo, J. E., Chabner, B. A. & Masur, H. (1988). *Antimicrob. Agents Chemother.* **32**, 430–433.
Lovell, S. C., Davis, I. W., Arendell, W. B. III, de Baker, P. L. W., Word, J. M., Prisant, M. G., Richardson, J. S. & Richardson, D. C. (2002). *Proteins*, **50**, 437–450.
McPhillips, T. M., McPhillips, S. E., Chiu, H.-J., Cohen, A. E., Deacon, A. M., Ellis, P. J., Garman, E., Gonzalez, A., Sauter, N. K., Phizackerley, R. P., Soltis, S. M. & Kuhn, P. (2002). *J. Synchrotron Rad.* **9**, 401–406.
Murshudov, G. N., Skubák, P., Lebedev, A. A., Pannu, N. S., Steiner, R. A., Nicholls, R. A., Winn, M. D., Long, F. & Vagin, A. A. (2011). *Acta Cryst.* D**67**, 355–367.
Vagin, A. & Teplyakov, A. (2010). *Acta Cryst.* D**66**, 22–25.
Winn, M. D. *et al.* (2011). *Acta Cryst.* D**67**, 235–242.